JOURNAL OF GUIDANCE, CONTROL, AND DYNAMICS
Vol. 35, No. 3, May–June 2012

Nonlinear Control Analysis of a Double-Gimbal Variable-Speed Control Moment Gyroscope

Daan Stevenson* and Hanspeter Schaub†
University of Colorado, Boulder, Colorado 80309-0431

DOI: 10.2514/1.56104

A single double-gimbal variable-speed control moment gyroscope is considered as a method for three-dimensional spacecraft attitude control. First, the system's equations of motion are developed, where gimbal and wheel accelerations are prescribed as control inputs. The resulting necessary motor torques as well as system energy rates are computed for verification. Next, a novel control algorithm is developed from the stability constraint for reference trajectory tracking. In contrast with the control development for single-gimbal variable-speed gyros, a Newton–Raphson scheme is required to solve for the desired double-gimbal variable-speed control moment gyroscope control variables because they appear in cross product and quadratic form, preventing analytical solutions. Analysis of the control theory suggests that the same torque amplification effects exist as in a single-gimbal control moment gyro, but control by a single double-gimbal variable-speed control moment gyroscope device is not robust due to potential configurations that result in control singularities. When these singularities are avoided, a simulation with successful reference trajectory tracking is achieved. Allowing double-gimbal gyros to have variable wheel speeds provides additional torquing capabilities, which is significant if failure modes are considered. As will be shown, a single double-gimbal variable-speed control moment gyroscope device can provide limited three-dimensional attitude control.

I. Introduction

MOMENTUM exchange devices have long been the preferred solution for long-term attitude control of spacecraft. The benefits over thrusters are that they do not expend nonrenewable fuel reserves nor expel caustic exhaust materials. Rather, momentum exchange devices require only electrical energy that is readily renewable with solar panels. A reaction wheel, the simplest momentum exchange device, can exert a torque on the spacecraft in a single orientation when its wheel speed is varied by the motor [1,2]. A single-gimbal control moment gyroscope (CMG) provides additional control by gimbaling a wheel spinning at a constant speed. This produces larger effective torques on the spacecraft but necessitates more complex control laws. While a CMG can easily encounter control singularities, a variable-speed CMG (VSCMG) introduces an extra degree of freedom that can be used to avoid these singularities, although it is similarly engineered [3–6].

The torque amplification mentioned above can be deduced mathematically by considering the equations of motion (EOM) of a VSCMG, as developed by Schaub et al. [7], Schaub and Junkins [8], and McMahon and Schaub [9]. The dominant angular momentum term is a cross-coupled term between the gimbal angle rate $\dot{\gamma}$ and the reaction wheel rotation rate Ω. When Ω is large, i.e., the reaction wheel is spun up, and $\dot{\gamma}$ is larger than the body angular rates $\boldsymbol{\omega}$, this term dominates the torquelike quantities in the EOM and significantly affects the spacecraft angular acceleration with a relatively small $\dot{\gamma}$. Since the expressions for the required motor torques do not contain this cross-coupled term, this mode of operation provides large torques on the spacecraft motion without exerting large amounts of energy.

Presented at the AAS/AIAA Astrodynamics Specialist Conference, Girdwood, AK, 31 July–4 August 2011; received 24 August 2011; revision received 6 December 2011; accepted for publication 9 December 2011.

*Graduate Research Assistant, Department of Aerospace Engineering Sciences. Member AIAA.

†Associate Professor, Department of Aerospace Engineering Sciences. Associate Fellow AIAA.

In the 1960s and 1970s, there was a research thrust to develop control laws for one or more double-gimbal CMGs with fixed wheel speed, which allows the flywheel to gimbal about two independent axes [10–13]. Such devices were used for attitude control on the Skylab space station and its Apollo Telescope Mount, and they have more recently been implemented on the International Space Station [14]. In contrast with single-gimbal CMGs, each device is capable of producing two torque vectors. However, this increased actuation capability comes at a price. The resulting large set of control torques of a cluster of double-gimbal devices can oppose each other, resulting in higher energy usage in contrast with single-gimbal devices. The benefit of such devices includes reduced issues with CMG singularities, as well as better capabilities to absorb external disturbance torques. The latter feature allows double-gimbal systems to operate longer before a momentum dumping maneuver is required. A drawback of both the variable-speed and double-gimbal CMGs is that they exhibit only two degrees of freedom, and a single such mechanism can therefore never provide full three-dimensional (3-D) attitude control. Moreover, the double-gimbal CMG control laws that are available in the literature [11,12] were developed neglecting inertia contributions from frame structures and motors, and they implemented momentum vector tracking with feedback servocontrol rather than complete nonlinear attitude control.

This paper proposes control of a spacecraft using a double-gimbal VSCMG (DGV) with a nonlinear attitude control strategy that accounts for the gimbal frame inertias. Since it contains three torque-producing motors, a single DGV allows for full control of the 3-D spacecraft attitude. The caveat is whether or not singularity configurations could occur as in the VSCMG. Furthermore, it is desired to determine mathematically whether the same torque amplification effects occur in a DGV. To answer these questions, the EOM and a control stability constraint of the device are developed. Then, a DGV feedback control method is created that avoids any local gimbal rate linearizations. Finally, the dynamics of a spacecraft with a single DGV system is simulated with a control law that uses both the gimbal torques and the reaction wheel mode of the device. The single DGV configuration is employed to illustrate the three-axis control capabilities and study the basic DGV control issues. Eventually, multi-DGV configurations would provide enhanced robustness to singular DGV configurations, as well as reduce the flywheel motor torque requirements. However, this paper illustrates that a single

double-gimbal CMG device can provide limited three-axis control in case a mechanical failure renders only a single device operable.

II. Double-Gimbal Variable-Speed Control Moment Gyroscope Equations Of Motion

Derivation of the EOM for the DGV is approached in an alternate way to the developments of [7]. In the single-gimbal case, the moments of inertia for each component are expressed in the same set of coordinates, which are rotated by the appropriate gimbal angle from the original orientation of the VSCMG. Because there are two gimbal angles in the DGV configuration, and the structure frames obtain different orientations, this approach does not simplify easily. Instead of taking inertial derivatives when applying Euler's equation, the transport theorem is more heavily used while extracting gimbal angles and rates from coordinate vectors to analyze the effect of various terms.

A representation of the DGV is shown in Fig. 1. The F frame defines the orientation of the entire device in the spacecraft body but stays fixed with respect to the craft, where $\hat{\boldsymbol{f}}_1$, $\hat{\boldsymbol{f}}_2$, and $\hat{\boldsymbol{f}}_3$ are the orthogonal unit vectors of frame F, and likewise for the other reference frames. Coordinate frame rotations to the G and H frames are given by Euler angle rotations through angles ψ and θ. Here, $[AB]$ is the direction cosine matrix that defines the orientation of the A frame relative to the B frame, and $[M_i(\alpha)]$ denotes a positive rotation by angle α about the ith axis. As such, if the gimbal angles are known at a given time, any unit vector $\hat{\boldsymbol{g}}_i$ or $\hat{\boldsymbol{h}}_i$ can be expressed in F frame coordinates by the relations

$$[GF] = [M_3(\psi)] \tag{1}$$

$$[HF] = [M_2(\theta)][M_3(\psi)] \tag{2}$$

and rotation to the spacecraft body frame is given by

$$[BF] = [\hat{\boldsymbol{f}}_1, \hat{\boldsymbol{f}}_2, \hat{\boldsymbol{f}}_3] \tag{3}$$

Now, the rotation of each frame with respect to the one outside it can be written in terms of these unit vectors and various angular rates:

$$\boldsymbol{\omega}_{B/N} = \boldsymbol{\omega} \tag{4}$$

$$\boldsymbol{\omega}_{G/B} = \dot{\psi}\hat{\boldsymbol{f}}_3 \tag{5}$$

$$\boldsymbol{\omega}_{H/G} = \dot{\theta}\hat{\boldsymbol{g}}_2 \tag{6}$$

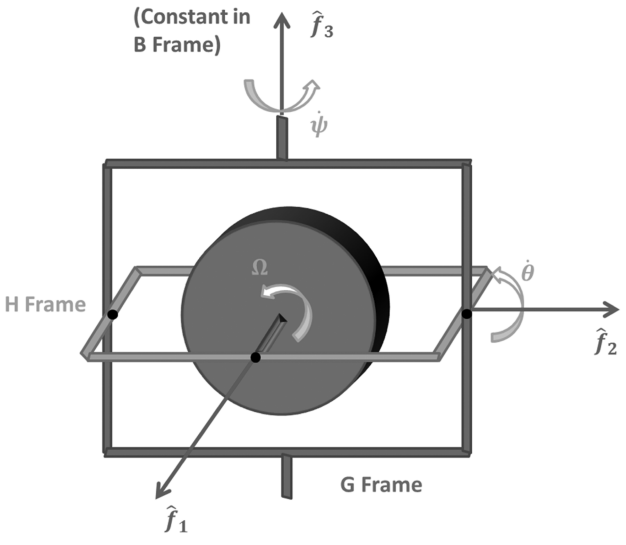

Fig. 1 Depiction of a DGV with coordinates and gimbal angles labeled.

$$\boldsymbol{\omega}_{W/H} = \Omega\hat{\boldsymbol{h}}_1 \tag{7}$$

These relations are used to solve for the time derivative of the angular momentum $\boldsymbol{H}_i$ of each spacecraft/device component i (spacecraft body B, the G and H structure frames, and the reaction wheel W) so that Euler's rotational EOM can be applied to the combined angular momentum $\boldsymbol{H}$ as follows:

$$\boldsymbol{H} = \boldsymbol{H}_B + \boldsymbol{H}_G + \boldsymbol{H}_H + \boldsymbol{H}_W \tag{8}$$

For the spacecraft body, there is the following well-known relation, using $[I_i]$ for the moment of inertia of component i about its center of mass:

$$\boldsymbol{H}_B = [I_S]\boldsymbol{\omega} \Rightarrow \dot{\boldsymbol{H}}_B = [I_S]\dot{\boldsymbol{\omega}} + \boldsymbol{\omega} \times [I_S]\boldsymbol{\omega} \tag{9}$$

For the other components, the derivation requires some more attention. Starting with the G structure frame,

$$\boldsymbol{H}_G = [I_G]\boldsymbol{\omega}_{G/N} = [I_G](\boldsymbol{\omega} + \dot{\psi}\hat{\boldsymbol{f}}_3) \tag{10}$$

By several iterations of the transport theorem, where $\frac{{}^i\mathrm{d}}{\mathrm{d}t}$ is used to define a frame-dependent time derivative with respect to frame i, Eq. (11) results. $[I_G]$ is removed from the derivative in the second line because it is constant in the G frame. The G frame derivative of $\boldsymbol{\omega}_{G/N}$ is equivalent to its N frame derivative, and finally, the transport theorem is used for the N frame derivative of $\dot{\psi}\hat{\boldsymbol{f}}_3$:

$$\begin{aligned}\dot{\boldsymbol{H}}_G &= \frac{{}^G\mathrm{d}}{\mathrm{d}t}([I_G]\boldsymbol{\omega}_{G/N}) + \boldsymbol{\omega}_{G/N} \times ([I_G]\boldsymbol{\omega}_{G/N}) \\ &= [I_G]\left(\frac{{}^N\mathrm{d}}{\mathrm{d}t}(\boldsymbol{\omega} + \dot{\psi}\hat{\boldsymbol{f}}_3)\right) + \boldsymbol{\omega}_{G/N} \times ([I_G]\boldsymbol{\omega}_{G/N}) \\ &= [I_G](\dot{\boldsymbol{\omega}} + \ddot{\psi}\hat{\boldsymbol{f}}_3 + \boldsymbol{\omega} \times (\dot{\psi}\hat{\boldsymbol{f}}_3)) + \boldsymbol{\omega}_{G/N} \times ([I_G]\boldsymbol{\omega}_{G/N})\end{aligned} \tag{11}$$

The same approach is taken for the H structure frame and the reaction wheel W to achieve

$$\boldsymbol{H}_H = [I_H]\boldsymbol{\omega}_{H/N} = [I_H](\boldsymbol{\omega} + \dot{\psi}\hat{\boldsymbol{f}}_3 + \dot{\theta}\hat{\boldsymbol{g}}_2) \tag{12}$$

$$\begin{aligned}\dot{\boldsymbol{H}}_H = [I_H](&\dot{\boldsymbol{\omega}} + \ddot{\psi}\hat{\boldsymbol{f}}_3 + \ddot{\theta}\hat{\boldsymbol{g}}_2 + \boldsymbol{\omega} \times (\dot{\psi}\hat{\boldsymbol{f}}_3 + \dot{\theta}\hat{\boldsymbol{g}}_2) + (\dot{\psi}\hat{\boldsymbol{f}}_3) \\ &\times (\dot{\theta}\hat{\boldsymbol{g}}_2)) + \boldsymbol{\omega}_{H/N} \times ([I_H]\boldsymbol{\omega}_{H/N})\end{aligned} \tag{13}$$

and

$$\boldsymbol{H}_W = [I_W]\boldsymbol{\omega}_{W/N} = [I_W](\boldsymbol{\omega} + \dot{\psi}\hat{\boldsymbol{f}}_3 + \dot{\theta}\hat{\boldsymbol{g}}_2 + \Omega\hat{\boldsymbol{h}}_1) \tag{14}$$

$$\begin{aligned}\dot{\boldsymbol{H}}_W = [I_W](&\dot{\boldsymbol{\omega}} + \ddot{\psi}\hat{\boldsymbol{f}}_3 + \ddot{\theta}\hat{\boldsymbol{g}}_2 + \dot{\Omega}\hat{\boldsymbol{h}}_1 + \boldsymbol{\omega} \times (\dot{\psi}\hat{\boldsymbol{f}}_3 + \dot{\theta}\hat{\boldsymbol{g}}_2 + \Omega\hat{\boldsymbol{h}}_1) \\ &+ (\dot{\psi}\hat{\boldsymbol{f}}_3) \times (\dot{\theta}\hat{\boldsymbol{g}}_2 + \Omega\hat{\boldsymbol{h}}_1) + (\dot{\theta}\hat{\boldsymbol{g}}_2) \times (\Omega\hat{\boldsymbol{h}}_1)) \\ &+ \boldsymbol{\omega}_{W/N} \times ([I_W]\boldsymbol{\omega}_{W/N})\end{aligned} \tag{15}$$

Since these equations all need to be expressed in body coordinates, the moment of inertia matrices need to be modified as follows from their diagonal measured form. The unit vectors are also to be expressed in body coordinates as discussed earlier:

$${}^B[I_G] = [BF][FG]^G[I_G][GF][FB] \tag{16}$$

$${}^B[I_H] = [BF][FH]^H[I_H][HF][FB] \tag{17}$$

$${}^B[I_W] = [BF][FH]^H[I_W][HF][FB] \tag{18}$$

The modified angular momentum derivatives $\dot{\boldsymbol{H}}'_i$ and combined moment of inertia $[I]$ are defined as

$$\dot{\boldsymbol{H}}'_i = \dot{\boldsymbol{H}}_i - [I_i]\dot{\boldsymbol{\omega}} \tag{19}$$

$$[I] = [I_S] + [I_G] + [I_H] + [I_W] \tag{20}$$

The full EOM of a DGV then become

$$[I]\dot{\boldsymbol{\omega}} = -\boldsymbol{\omega} \times [I_S]\boldsymbol{\omega} - \dot{\boldsymbol{H}}'_G - \dot{\boldsymbol{H}}'_H - \dot{\boldsymbol{H}}'_W + \boldsymbol{L} \tag{21}$$

Note that the gimbal rates can be isolated from every term in Eqs. (11), (13), and (15), because they are scalars. The cross-product terms also contain the gimbal rates, including cross-coupled term. These will be expanded for the control law derivation, resulting in further simplification that is not necessary for simulation of the EOM. If the DGV is not located at the center of mass of the spacecraft, the offcenter inertia components can be incorporated in the spacecraft inertia $[I_S]$ using the parallel axis theorem [15]. $[I_S]$ remains a constant matrix in the B frame even with the offcenter DGV inertia added, so Eq. (9) holds.

III. Equations of Motion Verification

The rotation of a spacecraft with one DGV is simulated by propagating the state vector $x = [\boldsymbol{\sigma}, \boldsymbol{\omega}, \psi, \dot{\psi}, \theta, \dot{\theta}, \Omega]^T$ using Eq. (21). Modified Rodriguez parameters (MRPs) are used to define the spacecraft attitude, denoted by $\boldsymbol{\sigma}$ [3,16,17]. The gimbal and wheel accelerations $\ddot{\psi}$, $\ddot{\theta}$, and $\dot{\Omega}$ are specified by a determined control law, assuming a servoloop is implemented by the motors. The resulting motor torques u_i on the wheel W, the H structure frame (inner gimbal), and the G structure frame (outer gimbal) can then be found by

$$[HF][FB]({}^B\dot{\boldsymbol{H}}_W) = {}^H\begin{bmatrix} u_W \\ \sim \\ \sim \end{bmatrix} \tag{22}$$

$$[GF][FB]({}^B\dot{\boldsymbol{H}}_H + {}^B\dot{\boldsymbol{H}}_W) = {}^G\begin{bmatrix} \sim \\ u_H \\ \sim \end{bmatrix} \tag{23}$$

$$[FB]({}^B\dot{\boldsymbol{H}}_G + {}^B\dot{\boldsymbol{H}}_H + {}^B\dot{\boldsymbol{H}}_W) = {}^F\begin{bmatrix} \sim \\ \sim \\ u_G \end{bmatrix} \tag{24}$$

A good check to see whether the simulation is running correctly is to compare the numerical derivate of the analytical kinetic energy equation (25) and the analytical expression for the kinetic energy rate equation (26) according to the work-energy-rate principle [15]:

$$T = \tfrac{1}{2}\boldsymbol{\omega}^T_{B/N}[I_S]\boldsymbol{\omega}_{B/N} + \tfrac{1}{2}\boldsymbol{\omega}^T_{G/N}[I_G]\boldsymbol{\omega}_{G/N} + \tfrac{1}{2}\boldsymbol{\omega}^T_{H/N}[I_H]\boldsymbol{\omega}_{H/N} + \tfrac{1}{2}\boldsymbol{\omega}^T_{W/N}[I_W]\boldsymbol{\omega}_{W/N} \tag{25}$$

$$\dot{T} = \boldsymbol{\omega}^T_{B/N}\boldsymbol{L} + \dot{\psi}u_G + \dot{\theta}u_H + \Omega u_W \tag{26}$$

Table 1 Parameters for EOM simulation with trivial control law

Parameter	Value	Units
${}^B[I_S]$	diag([50 150 100])	kg · m²
${}^G[I_G]$	diag([2 1 1])	kg · m²
${}^H[I_H]$	diag([1 1 2])	kg · m²
${}^H[I_W]$	diag([15 10 10])	kg · m²
$\boldsymbol{\sigma}(t_0)$	[0.4 −0.3 0.2]	
$\boldsymbol{\omega}(t_0)$	[−0.1 −0.05 0.2]	rad/s
$\dot{\psi}(t_0)$	0.03	rad/s
$\dot{\theta}(t_0)$	−0.01	rad/s
$\Omega(t_0)$	3	rad/s

The EOM were simulated using MATLAB®, with a control law specifying zero gimbal and wheel accelerations (so that the motors essentially maintain constant wheel speeds). The DGV is aligned with the spacecraft body principal axes, and gimbal angles start at zero while no external torques are present. The simulation parameters are given in Table 1, while Figs. 2 and 3 show the spacecraft motion, and the motor torques and energy rates. Figure 3b compares the numerical and analytic energy rates as mentioned above, which were found to match within expected numerical deviations. Note that the kinetic energy is expected to vary for a nonrigid spacecraft, even without external torques, because there are motors doing work on the DGV subcomponents.

IV. Control Theory

A. Stability Constraint

Now that the DGV EOM are verified, the next goal is to find a control law for the gimbal and wheel accelerations that achieves a

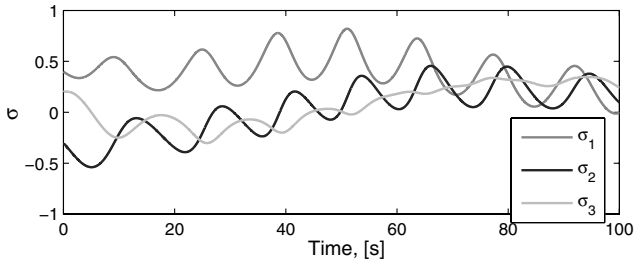

a) Attitude of spacecraft body (MRP)

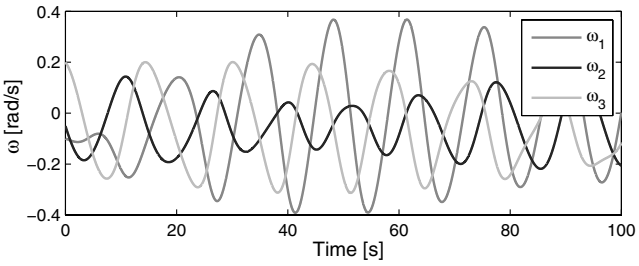

b) Angular velocity of spacecraft body

Fig. 2 Motion of spacecraft with gimbal and wheel accelerations held to zero.

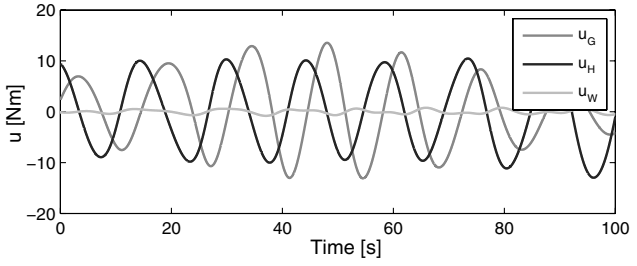

a) Motor torques

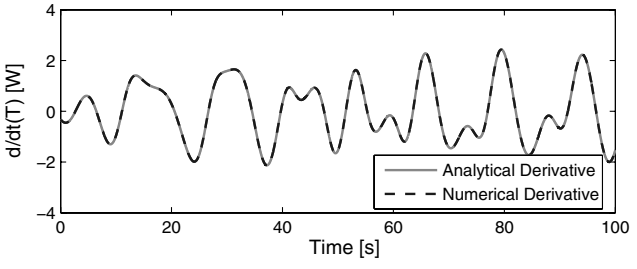

b) Kinetic energy rate of spacecraft

Fig. 3 Torques and energy rates with gimbal and wheel accelerations held to zero.

desired reference attitude. Where previous double-gimbal CMG control laws have used desired momentum vector tracking with feedback control to determine gimbal rates [11,12], a rigorous nonlinear Lyapunov control law is developed here. Just as in Schaub and Junkin's development of VSCMG control [15], Eq. (27) is a valid Lyapunov function for the DGV control dynamics if Eq. (28) is satisfied:

$$V(\delta\boldsymbol{\omega},\boldsymbol{\sigma}) = \tfrac{1}{2}\delta\boldsymbol{\omega}^T[I]\delta\boldsymbol{\omega} + 2K\ln(1+\boldsymbol{\sigma}^T\boldsymbol{\sigma}) \tag{27}$$

$$-[I]\dot{\boldsymbol{\omega}} - \frac{1}{2}\frac{{}^B\mathrm{d}}{\mathrm{d}t}[I]\delta\boldsymbol{\omega} = K\boldsymbol{\sigma} + [P]\delta\boldsymbol{\omega} - [I](\dot{\boldsymbol{\omega}}_r - \boldsymbol{\omega}\times\boldsymbol{\omega}_r) \tag{28}$$

where $\delta\boldsymbol{\omega} = \boldsymbol{\omega} - \boldsymbol{\omega}_r$ and $\boldsymbol{\sigma}$ denotes $\boldsymbol{\sigma}_{B/R}$, the MRPs of the current orientation relative to the desired orientation. For proper analysis, it is necessary to identify where the gimbal and wheel rates appear in this stability constraint. Equation (21) can be substituted for $[I]\dot{\boldsymbol{\omega}}$, but the body derivatives of the moments of inertia need to be resolved in order to identify further gimbal rate terms. Using the relations $[\dot{BN}] = -[{}^B\tilde{\boldsymbol{\omega}}_{B/N}][BN]$, ${}^B\boldsymbol{\omega}_{B/N} = -{}^B\boldsymbol{\omega}_{N/B}$, $[\dot{BN}]^T = [\dot{NB}]$, and $[\tilde{\boldsymbol{\omega}}]^T = -[\tilde{\boldsymbol{\omega}}]$, the following manipulations result:

$${}^B[I_G] = [BG]^G[I_G][GB] \tag{29}$$

$$\begin{aligned}\frac{{}^B\mathrm{d}}{\mathrm{d}t}[I_G] &= [{}^B\tilde{\boldsymbol{\omega}}_{G/B}][BG]^G[I_G][GB] - [BG]^G[I_G][GB][{}^B\tilde{\boldsymbol{\omega}}_{G/B}]\\ &= \dot{\psi}([\tilde{\hat{\boldsymbol{f}}}_3][I_G] - [I_G][\tilde{\hat{\boldsymbol{f}}}_3])\end{aligned} \tag{30}$$

where in the last line, the moments of inertia need to be expressed in body coordinates, as in the earlier development. The same approach yields the following:

$$\frac{{}^B\mathrm{d}}{\mathrm{d}t}[I_H] = \dot{\psi}([\tilde{\hat{\boldsymbol{f}}}_3][I_H] - [I_H][\tilde{\hat{\boldsymbol{f}}}_3]) + \dot{\theta}([\tilde{\hat{\boldsymbol{g}}}_2][I_H] - [I_H][\tilde{\hat{\boldsymbol{g}}}_2]) \tag{31}$$

$$\begin{aligned}\frac{{}^B\mathrm{d}}{\mathrm{d}t}[I_W] &= \dot{\psi}([\tilde{\hat{\boldsymbol{f}}}_3][I_W] - [I_W][\tilde{\hat{\boldsymbol{f}}}_3]) + \dot{\theta}([\tilde{\hat{\boldsymbol{g}}}_2][I_W] - [I_W][\tilde{\hat{\boldsymbol{g}}}_2])\\ &\quad + \Omega([\tilde{\hat{\boldsymbol{h}}}_1][I_W] - [I_W][\tilde{\hat{\boldsymbol{h}}}_1])\end{aligned} \tag{32}$$

Using the combined moment of inertia matrices $[I_{GHW}] = [I_G] + [I_H] + [I_W]$ and $[I_{HW}] = [I_H] + [I_W]$, and expanding all terms including the cross products in the modified angular momentum derivatives, Eq. (28) can be rewritten as follows, where the gimbal and wheel rates and accelerations are factored out from the other expressions:

$$\begin{aligned}&\ddot{\psi}\{[I_{GHW}]\hat{\boldsymbol{f}}_3\} + \ddot{\theta}\{[I_{HW}]\hat{\boldsymbol{g}}_2\} + \dot{\Omega}\{[I_W]\hat{\boldsymbol{h}}_1\}\\
&\quad + \dot{\psi}\{\tfrac{1}{2}[I_{GHW}](\boldsymbol{\omega}\times\hat{\boldsymbol{f}}_3) + \tfrac{1}{2}\hat{\boldsymbol{f}}_3\times([I_{GHW}]\boldsymbol{\omega}) + \boldsymbol{\omega}\times([I_{GHW}]\hat{\boldsymbol{f}}_3)\\
&\quad + \tfrac{1}{2}\hat{\boldsymbol{f}}_3\times([I_{GHW}]\delta\boldsymbol{\omega}) + \tfrac{1}{2}[I_{GHW}](\delta\boldsymbol{\omega}\times\hat{\boldsymbol{f}}_3)\}\\
&\quad + \dot{\theta}\{\tfrac{1}{2}[I_{HW}](\boldsymbol{\omega}\times\hat{\boldsymbol{g}}_2) + \tfrac{1}{2}\hat{\boldsymbol{g}}_2\times([I_{HW}]\boldsymbol{\omega}) + \boldsymbol{\omega}\times([I_{HW}]\hat{\boldsymbol{g}}_2)\\
&\quad + \tfrac{1}{2}\hat{\boldsymbol{g}}_2\times([I_{HW}]\delta\boldsymbol{\omega}) + \tfrac{1}{2}[I_{HW}](\delta\boldsymbol{\omega}\times\hat{\boldsymbol{g}}_2)\}\\
&\quad + \Omega\{\tfrac{1}{2}[I_W](\boldsymbol{\omega}\times\hat{\boldsymbol{h}}_1) + \tfrac{1}{2}\hat{\boldsymbol{h}}_1\times([I_W]\boldsymbol{\omega}) + \boldsymbol{\omega}\times([I_W]\hat{\boldsymbol{h}}_1)\\
&\quad + \tfrac{1}{2}\hat{\boldsymbol{h}}_1\times([I_W]\delta\boldsymbol{\omega}) + \tfrac{1}{2}[I_W](\delta\boldsymbol{\omega}\times\hat{\boldsymbol{h}}_1)\}\\
&\quad + \dot{\psi}\,\dot{\theta}\{[I_{HW}](\hat{\boldsymbol{f}}_3\times\hat{\boldsymbol{g}}_2) + \hat{\boldsymbol{f}}_3\times([I_{HW}]\hat{\boldsymbol{g}}_2) + \hat{\boldsymbol{g}}_2\times([I_{HW}]\hat{\boldsymbol{f}}_3)\}\\
&\quad + \dot{\psi}\Omega\{[I_W](\hat{\boldsymbol{f}}_3\times\hat{\boldsymbol{h}}_1) + \hat{\boldsymbol{f}}_3\times([I_W]\hat{\boldsymbol{h}}_1) + \hat{\boldsymbol{h}}_1\times([I_W]\hat{\boldsymbol{f}}_3)\}\\
&\quad + \dot{\theta}\Omega\{[I_W](\hat{\boldsymbol{g}}_2\times\hat{\boldsymbol{h}}_1) + \hat{\boldsymbol{g}}_2\times([I_W]\hat{\boldsymbol{h}}_1) + \hat{\boldsymbol{h}}_1\times([I_W]\hat{\boldsymbol{g}}_2)\}\\
&\quad + \dot{\psi}^2\{\hat{\boldsymbol{f}}_3\times([I_{GHW}]\hat{\boldsymbol{f}}_3)\} + \dot{\theta}^2\{\hat{\boldsymbol{g}}_2\times([I_{HW}]\hat{\boldsymbol{g}}_2)\}\\
&\quad + \Omega^2\{\hat{\boldsymbol{h}}_1\times([I_W]\hat{\boldsymbol{h}}_1)\}\\
&\quad = K\boldsymbol{\sigma} + [P]\delta\boldsymbol{\omega} + \boldsymbol{L} - \boldsymbol{\omega}\times([I]\boldsymbol{\omega}) - [I](\dot{\boldsymbol{\omega}}_r - \boldsymbol{\omega}\times\boldsymbol{\omega}_r)\end{aligned} \tag{33}$$

Equation (33) can be simplified by some mathematical cancellations and further approximations. First, the coefficient of Ω^2, $\{\hat{\boldsymbol{h}}_1\times([I_W]\hat{\boldsymbol{h}}_1)\}$, is found to be zero when computed in the H frame, and the same reasoning results in a zero coefficient of $\dot{\theta}^2$. Next, the gimbal accelerations $\ddot{\psi}$ and $\ddot{\theta}$ are assumed to be very small and neglected in the remainder of the derivation. Since these accelerations are prescribed by the control law, it is possible to ensure they remain small. As in the case of a VSCMG, implementing a velocity-based control law ensures that both the reaction wheel mode and the torque amplification effect of the gimbals are used [7–9]. As such, desired $\dot{\psi}$, $\dot{\theta}$, and $\dot{\Omega}$ are computed to satisfy Eq. (33). The only remaining term on the left-hand side that is not used to solve for control parameters then is the Ω term, and just like in the VSCMG derivation, it is feedback-compensated and included in the desired torque $\boldsymbol{L}_r$ to be exerted on the spacecraft body by the DGV [15]. The following finalized Lyapunov control stability constraint is obtained:

$$\begin{aligned}&\dot{\Omega}\{[I_W]\hat{\boldsymbol{h}}_1\}\\
&\quad + \dot{\psi}\{\tfrac{1}{2}[I_{GHW}](\boldsymbol{\omega}\times\hat{\boldsymbol{f}}_3) + \tfrac{1}{2}\hat{\boldsymbol{f}}_3\times([I_{GHW}]\boldsymbol{\omega}) + \boldsymbol{\omega}\times([I_{GHW}]\hat{\boldsymbol{f}}_3)\\
&\quad + \tfrac{1}{2}\hat{\boldsymbol{f}}_3\times([I_{GHW}]\delta\boldsymbol{\omega}) + \tfrac{1}{2}[I_{GHW}](\delta\boldsymbol{\omega}\times\hat{\boldsymbol{f}}_3)\\
&\quad + \Omega([I_W](\hat{\boldsymbol{f}}_3\times\hat{\boldsymbol{h}}_1) + \hat{\boldsymbol{f}}_3\times([I_W]\hat{\boldsymbol{h}}_1) + \hat{\boldsymbol{h}}_1\times([I_W]\hat{\boldsymbol{f}}_3))\}\\
&\quad + \dot{\theta}\{\tfrac{1}{2}[I_{HW}](\boldsymbol{\omega}\times\hat{\boldsymbol{g}}_2) + \tfrac{1}{2}\hat{\boldsymbol{g}}_2\times([I_{HW}]\boldsymbol{\omega}) + \boldsymbol{\omega}\times([I_{HW}]\hat{\boldsymbol{g}}_2)\\
&\quad + \tfrac{1}{2}\hat{\boldsymbol{g}}_2\times([I_{HW}]\delta\boldsymbol{\omega}) + \tfrac{1}{2}[I_{HW}](\delta\boldsymbol{\omega}\times\hat{\boldsymbol{g}}_2)\\
&\quad + \Omega([I_W](\hat{\boldsymbol{g}}_2\times\hat{\boldsymbol{h}}_1) + \hat{\boldsymbol{g}}_2\times([I_W]\hat{\boldsymbol{h}}_1) + \hat{\boldsymbol{h}}_1\times([I_W]\hat{\boldsymbol{g}}_2))\}\\
&\quad + \dot{\psi}\,\dot{\theta}\{[I_{HW}](\hat{\boldsymbol{f}}_3\times\hat{\boldsymbol{g}}_2) + \hat{\boldsymbol{f}}_3\times([I_{HW}]\hat{\boldsymbol{g}}_2) + \hat{\boldsymbol{g}}_2\times([I_{HW}]\hat{\boldsymbol{f}}_3)\}\\
&\quad + \dot{\psi}^2\{\hat{\boldsymbol{f}}_3\times([I_{GHW}]\hat{\boldsymbol{f}}_3)\}\\
&\quad = K\boldsymbol{\sigma} + [P]\delta\boldsymbol{\omega} + \boldsymbol{L} - \boldsymbol{\omega}\times([I]\boldsymbol{\omega}) - [I](\dot{\boldsymbol{\omega}}_r - \boldsymbol{\omega}\times\boldsymbol{\omega}_r)\\
&\quad - \Omega\{\tfrac{1}{2}[I_W](\boldsymbol{\omega}\times\hat{\boldsymbol{h}}_1) + \tfrac{1}{2}\hat{\boldsymbol{h}}_1\times([I_W]\boldsymbol{\omega}) + \boldsymbol{\omega}\times([I_W]\hat{\boldsymbol{h}}_1)\\
&\quad + \tfrac{1}{2}\hat{\boldsymbol{h}}_1\times([I_W]\delta\boldsymbol{\omega}) + \tfrac{1}{2}[I_W](\delta\boldsymbol{\omega}\times\hat{\boldsymbol{h}}_1)\} = \boldsymbol{L}_r\end{aligned} \tag{34}$$

This result can be rigorously compared with and verified by the stability constraint for a single-gimbal VSCMG. Setting $\dot{\theta}$ and $[I_H]$ to zero essentially removes the inside gimbal from the DGV, resulting in the same configuration as Schaub and Junkin's VSCMG development [15]. Now, the H frame coincides with the G frame, in which $[I_G]$ and $[I_W]$ are both diagonal. As a result, these moments of inertia are removed from many of the cross products in Eq. (34), and the terms on the left-hand side that do not vanish because of the zeroed control variables reduce to the corresponding formulations in the VSCMG stability constraint. The right-hand side of Eq. (34), or the required torque vector $\boldsymbol{L}_r$, also agrees directly with the VSCMG derivation.

If the second gimbal rotation is reinstated, it is evident that the stability relation contains the quadratic terms $\dot{\psi}\,\dot{\theta}$ and $\dot{\psi}^2$ that are not apparent in the constraint for a single-gimbal VSCMG. While this outcome holds even if wheel speed is fixed, it is not evident in the previous double-gimbal CMG developments because of simplifications in the EOM and control law formulations [12,13]. Because of the quadratic terms, solving for the control variables becomes less trivial than a simple matrix inversion, as will be discussed in the next section.

B. Control Algorithm

With the control stability constraint verified, it is used to solve for a desired $\dot{\psi}$, $\dot{\theta}$, and $\dot{\Omega}$ the control variables on the left-hand side of Eq. (34). Let us simplify the constraint by grouping the coefficient vectors of the control variables as the vectors $\boldsymbol{a}$ through $\boldsymbol{e}$:

$$\dot{\Omega}_{\mathrm{des}}\boldsymbol{a} + \dot{\psi}_{\mathrm{des}}\boldsymbol{b} + \dot{\theta}_{\mathrm{des}}\boldsymbol{c} + \dot{\psi}_{\mathrm{des}}\dot{\theta}_{\mathrm{des}}\boldsymbol{d} + \dot{\psi}^2_{\mathrm{des}}\boldsymbol{e} = \boldsymbol{L}_r \tag{35}$$

Using the control vector $\boldsymbol{u} = [\,\dot{\Omega}_{\mathrm{des}} \quad \dot{\psi}_{\mathrm{des}} \quad \dot{\theta}_{\mathrm{des}}\,]^T$, this becomes

$$[R]\boldsymbol{u} + \boldsymbol{u}^T[S]\boldsymbol{u} = \boldsymbol{L}_r \tag{36}$$

where matrices $[R]$ and $[S]$ are $[3 \times 1]$ and $[3 \times 3]$, respectively, but their entries are $[3 \times 1]$ vectors as follows:

$$[R] = [\, \boldsymbol{a} \quad \boldsymbol{b} \quad \boldsymbol{c} \,] \tag{37}$$

$$[S] = \begin{bmatrix} \boldsymbol{0} & \boldsymbol{0} & \boldsymbol{0} \\ \boldsymbol{0} & \boldsymbol{e} & \frac{1}{2}\boldsymbol{d} \\ \boldsymbol{0} & \frac{1}{2}\boldsymbol{d} & \boldsymbol{0} \end{bmatrix} \tag{38}$$

This nonlinear matrix equation cannot be solved analytically for $\boldsymbol{u}$; instead, a Newton–Raphson (N–R) iteration is used to find the root of the relation

$$\boldsymbol{f}(\boldsymbol{u}) = [R]\boldsymbol{u} + \boldsymbol{u}^T[S]\boldsymbol{u} - \boldsymbol{L}_r \tag{39}$$

For the initial guess, the control vector is solved with the quadratic terms neglected:

$$\boldsymbol{u}_0 = [R]^{-1}\boldsymbol{L}_r \tag{40}$$

Incremental corrections are made until the error $|\boldsymbol{f}(\boldsymbol{u})|$ is sufficiently small using

$$\boldsymbol{u} = \boldsymbol{u}_0 - [J]^{-1}\boldsymbol{f}(\boldsymbol{u}) \tag{41}$$

where $[J]$ is the Jacobian of $\boldsymbol{f}$ with $\boldsymbol{u}$:

$$[J] = [\, \boldsymbol{a} \quad \boldsymbol{b} + u_3\boldsymbol{d} + 2u_2\boldsymbol{e} \quad \boldsymbol{c} + u_2\boldsymbol{d} \,] \tag{42}$$

In the numerical control simulation presented later in this paper, where no singularities are encountered, the initial error $|\boldsymbol{f}(\boldsymbol{u}_0)|$ stays almost three orders of magnitude below the required torque size $|\boldsymbol{L}_r|$, and no more than two iterations are required to achieve an accuracy of 10^{-9} N · m in $|\boldsymbol{f}(\boldsymbol{u})|$. When singularities are not avoided, the amount of necessary iterations can become much larger.

The wheel acceleration from the control vector $\boldsymbol{u}$ can be implemented directly in the motor servo, but to determine the desired gimbal accelerations for their motor servos, a proportional control with feedforward term is required:

$$\dot{\Omega}_{\text{srv}} = \dot{\Omega}_{\text{des}} \tag{43}$$

$$\ddot{\psi}_{\text{srv}} = -K_{\dot{\psi}}(\dot{\psi} - \dot{\psi}_{\text{des}}) + \ddot{\psi}_{\text{des}} \tag{44}$$

$$\ddot{\theta}_{\text{srv}} = -K_{\dot{\theta}}(\dot{\theta} - \dot{\theta}_{\text{des}}) + \ddot{\theta}_{\text{des}} \tag{45}$$

where

$$\ddot{\psi}_{\text{des}} = \frac{\dot{\psi}_{\text{des}}(t) - \dot{\psi}_{\text{des}}(t - t_{\text{step}})}{t_{\text{step}}} \tag{46}$$

$$\ddot{\theta}_{\text{des}} = \frac{\dot{\theta}_{\text{des}}(t) - \dot{\theta}_{\text{des}}(t - t_{\text{step}})}{t_{\text{step}}} \tag{47}$$

As with CMG gimbal rate servocontrols solutions, exact control is not expected with this steering law because of the gimbal acceleration terms that are neglected. The best results are achieved when gimbal accelerations $\ddot{\boldsymbol{\psi}}$ and $\ddot{\boldsymbol{\theta}}$ are kept small, a similar requirement as for effective CMG control.

C. Control Singularities

The dominant terms from Eq. (33) that appear in the steering law are

$$\begin{aligned} &\dot{\Omega}\{[I_W]\hat{\boldsymbol{h}}_1\} + \dot{\psi}\Omega\{[I_W](\hat{\boldsymbol{f}}_3 \times \hat{\boldsymbol{h}}_1) + \hat{\boldsymbol{f}}_3 \times ([I_W]\hat{\boldsymbol{h}}_1) \\ &\quad + \hat{\boldsymbol{h}}_1 \times ([I_W]\hat{\boldsymbol{f}}_3)\} + \dot{\theta}\Omega\{[I_W](\hat{\boldsymbol{g}}_2 \times \hat{\boldsymbol{h}}_1) + \hat{\boldsymbol{g}}_2 \times ([I_W]\hat{\boldsymbol{h}}_1) \\ &\quad + \hat{\boldsymbol{h}}_1 \times ([I_W]\hat{\boldsymbol{g}}_2)\} \end{aligned} \tag{48}$$

The second two lines are equivalent to the torque amplification term in the VSCMG control law, since a small gimbal rate can produce a large torque quantity when Ω is large. If the operations in Eq. (48) are performed in the H frame, and the wheel moment of inertia matrix is expressed as

$${}^{H}[I_W] = \begin{bmatrix} I_{W_1} & 0 & 0 \\ 0 & I_{W_2} & 0 \\ 0 & 0 & I_{W_3} \end{bmatrix} \tag{49}$$

the result is

$$\begin{aligned} &\dot{\Omega} I_{W_2}\hat{\boldsymbol{h}}_1 + \dot{\psi}\Omega(I_{W_1} + I_{W_2} + I_{W_3})\cos\theta\hat{\boldsymbol{h}}_2 \\ &\quad - \dot{\theta}\Omega(I_{W_1} + I_{W_2} + I_{W_3})\hat{\boldsymbol{h}}_3 \end{aligned} \tag{50}$$

It is evident here that the dominant terms of this steering law span the entire vector space, except when $\theta = 90$ deg and the $\dot{\psi}\Omega$ term vanishes. This is logical because, at that configuration, the two gimbal frames line up and the torques from the outer gimbal motor and the wheel motor are collinear. There are other terms in the $\boldsymbol{a}$ vector of Eq. (36), but they do not contain Ω and are thus much smaller. The inclusion of the $\dot{\psi}\,\dot{\theta}$ term in the control law does not alleviate the singularity problem either because its associated vector can be shown to contain only components in the $\hat{\boldsymbol{h}}_1$ and $\hat{\boldsymbol{h}}_3$ directions. There is a chance the system pushes through this singularity, but the steering law is certainly not robust with a single DGV as there is no null space to avoid the singularity. Combined with another simple control device, such as a reaction wheel to avoid singularities, a single DGV could still provide effective spacecraft attitude control.

D. Control Simulation

The control law discussed above is implemented to track an arbitrary sinusoidal attitude reference trajectory. Spacecraft parameters and initial conditions are the same as in Table 1 with the exception of $\Omega(t_0)$ and the control parameters that are shown in Table 2.

Figure 4 shows that the velocity-based steering law does a very successful job of tracking the desired attitude, as long as singularities where θ approaches ± 90 deg are avoided. It is evident from Fig. 5a that this is the case with these simulation parameters (wheel speed is not shown, but it stays close to 100 rad/s). In the beginning of the simulation, the control law requires large motor torques to correct the initial attitude and velocity errors. In reality, the motors might saturate from this aggressive control, in which case time-dependent gains could be implemented to keep the desired servo accelerations within certain bounds.

As the gimbal frames approach the orientation where they are lined up, their motors see higher torques to resist each others' motion. This can be seen in the simulation in Fig. 6a, where u_G and u_W increase

Table 2 Parameters for reference tracking simulation with nonlinear control law

Parameter	Value	Units
$\Omega(t_0)$	100	rad/s
K	100	
$[P]$	diag([100 100 100])	
$K_{\dot{\psi}}$	10	
$K_{\dot{\theta}}$	10	

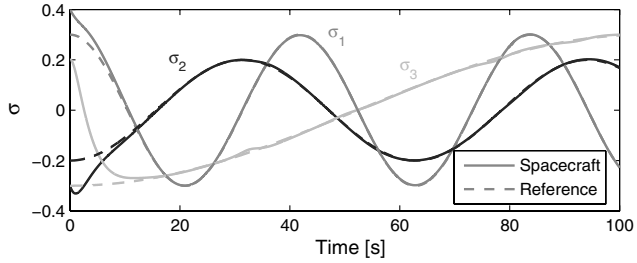

a) Attitude of spacecraft body (MRP)

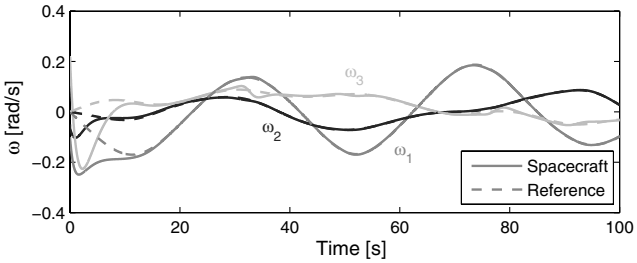

b) Angular velocity of spacecraft body

Fig. 4 Motion of spacecraft and reference trajectory with velocity-based steering law.

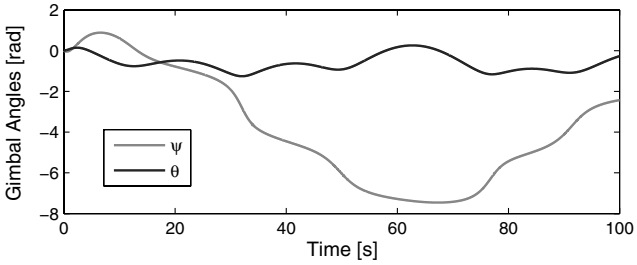

a) Gimbal angles

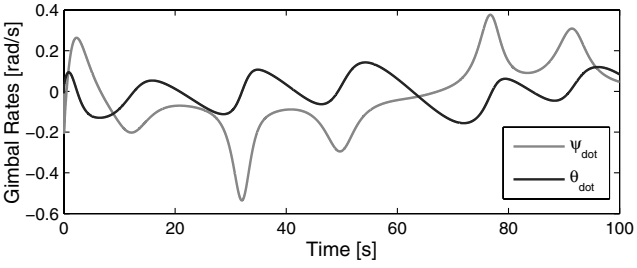

b) Gimbal rates

Fig. 5 Gimbal and wheel angles and rates with velocity-based steering law.

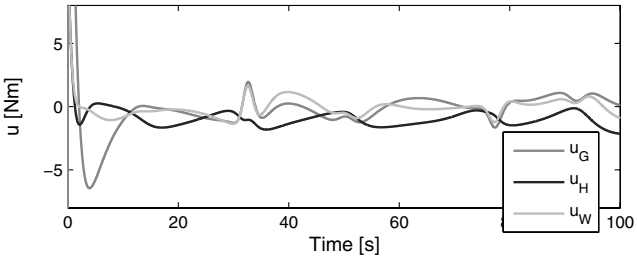

a) Motor torques

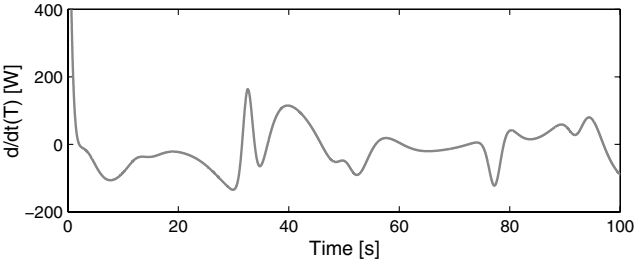

b) Kinetic energy rate of spacecraft

Fig. 6 Torques and spacecraft energy rates with velocity-based steering law.

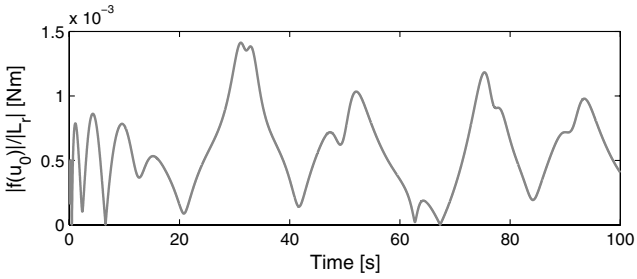

a) Percent error in initial newton-raphson guess for L_r

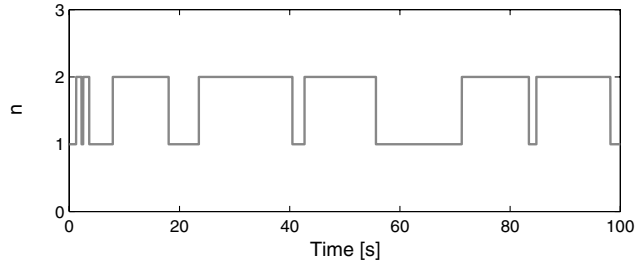

b) Number of newton-raphson iterations

Fig. 7 N–R initial guess error and number of iterations.

together and decrease together at roughly 35 and 80 s, respectively. This coincides with θ nearing -90 deg in Fig. 5a.

The error in the initial N–R guess, $|\boldsymbol{f}(\boldsymbol{u}_0)|$, and the number of iterations required to bring this error down to 10^{-9} N · m are shown in Fig. 7. Thus, while the control formulation requires iterating numerically to solve for DGV control variables from a quadratic matrix equation, this process is achieved very rapidly with only one to two iteration steps. Moreover, the errors in the computed desired torque stay within 0.15% without N–R iteration, suggesting that acceptable control would be achieved in this simulation without consideration of the quadratic control parameter terms. The computational cost of the N–R iteration represents only 2.08% of the control update calculation time, so there is no large detriment to determining the exact solution. When the DGV system approaches a singularity, however, the error and N–R iterations quickly increase, and more benefit is achieved by solving for the nonlinear parameters. In a flight-ready satellite, however, other actuators would be included to ensure that control singularities are avoided.

V. Conclusions

The goal of this investigation is to derive the full EOM of a DGV and determine whether a single such device can provide full attitude control of a spacecraft and employ the torque amplification seen in single-gimbal devices. The control law dynamics show that this torque amplification is indeed evident, but the DGV can encounter control singularities that prevent robust control from a single DGV device alone. The nonlinear nature of the stability constraint requires a novel approach in the control algorithm, namely, using a N–R solving method to acquire the desired control parameters. Since high accuracy resulted with only two iterations from the initial control guess using feedback compensation of the nonlinear terms, it is deduced that the coefficients of the nonlinear terms are generally small. When singularities where the gimbal frames line up with each other are avoided, the nonlinear control algorithm achieves very accurate tracking of a reference attitude trajectory. Future work will attempt to achieve robust control and singularity avoidance with a

multi-DGV cluster, using the null space that results from the system's extra degrees of freedom.

Acknowledgment

This material is based upon work supported by the National Science Foundation Graduate Research Fellowship under grant number (1000100047).

References

[1] Tsiotras, P., Shen, H., and Hall, C., "Satellite Attitude Control and Power Tracking with Energy/Momentum Wheels," *Journal of Guidance, Control, and Dynamics*, Vol. 24, No. 1, 2001, pp. 23–24. doi:10.2514/2.4705

[2] Richie, D. J., Lappas, V. J., and Prassinos, G., "Sizing/Optimization of a Small Satellite Energy Storage and Attitude Control System," *Journal of Spacecraft and Rockets*, Vol. 44, No. 4, July–Aug. 2007, pp. 940–952. doi:10.2514/1.25134

[3] Schaub, H., "Novel Coordinates for Nonlinear Multibody Motion with Applications to Spacecraft Dynamics and Control," Ph.D. Dissertation, Texas A & M Univ., College Station, TX, 1998.

[4] Yoon, H., and Tsiotras, P., "Spacecraft Adaptive Attitude and Power Tracking with Variable Speed Control Moment Gyroscopes," *Journal of Guidance, Control, and Dynamics*, Vol. 25, No. 6, 2002, pp. 1081–1090. doi:10.2514/2.4987

[5] Yoon, H., and Tsiotras, P., "Singularity Analysis of Variable Speed Control Moment Gyros," *Journal of Guidance, Control, and Dynamics*, Vol. 27, No. 3, 2004, pp. 374–386. doi:10.2514/1.2946

[6] Richie, D. J., Lappas, V. J., and Prassinos, G., "A Practical Small Satellite Variable-Speed Control Moment Gyroscope For Combined Energy Storage and Attitude Control," AAS/AIAA Astrodynamics Specialist Conference, Honolulu, HI, AIAA Paper 2008-7503, 18–21 Aug. 2008.

[7] Schaub, H., R. Vadali, S., and Junkins, J. L., "Feedback Control Law for Variable Speed Control Moment Gyroscopes," *Journal of the Astronautical Sciences*, Vol. 46, No. 3, July–Sept. 1998, pp. 307–328.

[8] Schaub, H., and Junkins, J. L., "Singularity Avoidance Using Null Motion and Variable-Speed Control Moment Gyros," *Journal of Guidance, Control, and Dynamics*, Vol. 23, No. 1, Jan.–Feb. 2000, pp. 11–16. doi:10.2514/2.4514

[9] McMahon, J., and Schaub, H., "Simplified Singularity Avoidance Using Variable Speed Control Moment Gyroscope Nullmotion," AAS/AIAA Spaceflight Mechanics Meeting, San Diego, CA, American Astronautical Soc. Paper 10-210, Springfield, VA, 14–18 Feb. 2010.

[10] O'Conner, B. J., and Morine, L., "A Description of the CMG and its Application to Space Vehicle Control," *Journal of Spacecraft and Rockets*, Vol. 6, No. 3, 1969, pp. 225–231. doi:10.2514/3.29577

[11] Kennel, H. F., "A Control Law for Double-Gimbaled Control Moment Gyros Used for Space Vehicle Attitude Control," NASA TM X-64536, 7 Aug. 1970.

[12] Kennel, H. F., "Steering Law for Parallel Mounted Double-Gimbaled Control Moment Gyros," NASA TM X-64930, Feb. 1975.

[13] Ahmed, J., and Bernstein, D., "Adaptive Control of Double-Gimbal Control-Moment Gyro with Unbalanced Rotor," *Journal of Guidance, Control, and Dynamics*, Vol. 25, No. 1, Jan.–Feb. 2002, pp. 105–115. doi:10.2514/2.4855

[14] Gurrisi, C., Seidel, R., Dickerson, S., Didziulis, S., Frantz, P., and Ferguson, K., "Space Station Control Moment Gyroscope Lessons Learned," *Proceedings of the 40th Aerospace Mechanisms Symposium*, NASA NASA/CP-2010-216272, Kennedy Space Center, 12–14 May 2010.

[15] Schaub, H., and Junkins, J. L., *Analytical Mechanics of Space Systems*, 2nd ed., AIAA Education Series, AIAA, Reston, VA, Oct. 2009, pp. 178–188, 408–430.

[16] Schaub, H., and Junkins, J. L., "Stereographic Orientation Parameters for Attitude Dynamics: A Generalization of the Rodrigues Parameters," *Journal of the Astronautical Sciences*, Vol. 44, No. 1, 1996, pp. 1–19.

[17] Schaub, H., and Junkins, J. L., "MATLAB Toolbox for Rigid Body Kinematics," Proceedings of the AAS/AIAA Space Flight Mechanics Meeting, Breckenridge, CO, American Astronautical Soc. Paper 99-139, Springfield, VA, 7–10 Feb. 1999, pp. 549–560.